Spin dynamics and damping in nanomagnets measured directly by frequency-resolved magneto-optic Kerr effect[a]

M. L. Schneider,[b] J. M. Shaw, A. B. Kos, Th. Gerrits, and T. J. Silva
National Institute of Standards and Technology, Boulder, Colorado 80303, USA

R. D. McMichael
National Institute of Standards and Technology, Gaithersburg, Maryland 20899, USA

The spin dynamics of sub-100-nm $Ni_{80}Fe_{20}$ nanomagnets are directly measured using the magneto-optic Kerr effect and a broadband detection scheme. Elliptical dots approximately 68 nm in diameter and 10 nm thick were fabricated in 20×20 μm^2 arrays. There is approximately a factor of 2 increase in the effective linewidth when compared to a 20 μm diameter continuous disk of the same material. Using micromagnetic simulations, we model the effect of dot-to-dot size variation on the effective linewidth and find that 2 nm size variations are more than sufficient to account for the effective increase in linewidth. [DOI: 10.1063/1.2812541]

I. INTRODUCTION

Current research in nanomagnetism extends from the spin transfer effects in confined systems,[1] to patterned bit recording media,[2] and to molecular nanomagnets.[3–5] The magnetic damping behavior of nanomagnets is important for patterned recording media and application in spin momentum transfer. Enhancement of the Gilbert damping parameter by a factor of 2 in the more complicated multilayer systems has been previously reported.[6–8] Proposed explanations for the enhanced damping have included an antiferromagnetic coupling to a native oxide,[8] the influence of nonequilibrium spin pumping effects,[9–12] the imperfections present in the edges, which make up a relatively large percentage of the total volume of the nanomagnets,[12,13] and effects of coupling to neighboring nanomagnets when the measurement is performed on an array.[14]

Dynamical properties of microarrays of nanodots are measured with a broadband optical measurement technique. We concentrate on arrays of elliptical nanodots 10 nm thick with 71 nm major and 65 nm minor axes. To verify repeatability, we performed measurements on several identically processed samples. The resonance frequencies of the arrays are consistent with expectations for ferromagnetic resonance (FMR) in ellipsoidal particles, as well as micromagnetic simulations of a single nanodot. Fits to the data yield a Gilbert damping parameter of $\alpha = 0.011 \pm 0.002$ for the arrays of nanodots independent of the presence or absence of a surface oxide.

II. EXPERIMENT

The measurement method presented here is an optical version of standard, broadband, and ferromagnetic resonance.[15,16] We use a broadband optical detection scheme based on the magneto-optic Kerr effect (MOKE). In this technique, the nanomagnets are excited by continuous microwaves traveling down a coplanar waveguide with a center conductor that is much larger than the nanomagnet array. A continuous wave 532 nm laser is focused and reflected off the surface of the nanomagnet array in the longitudinal MOKE configuration with respect to the microwave excitations. A static bias field is applied transverse to the plane of incidence. We are sensitive to motion of the magnetic moment both in the film plane parallel to the applied rf field and perpendicular to the film plane via the longitudinal and polar Kerr effects, respectively. A broadband detector (100 kHz–12 GHz bandwidth) is used to resolve the magnetic motion directly in the frequency domain. A vector network analyzer is used both to supply the microwave excitation and to read the corresponding intensity at the excitation frequency of the broadband detector. We apply a static bias field to the nanomagnet array and sweep the microwave frequency. To improve the sensitivity of the measurements, the system background, which is measured at the maximum applied bias field of 350 kA/m, is subtracted.

The films used for the samples were dc magnetron sputtered in Ar on sapphire substrates in an applied dc field to induce a uniaxial anisotropy. A 3 nm Ta seed layer was deposited followed by a 10 nm $Ni_{80}Fe_{20}$ (Permalloy) layer at 0.33 Pa. Some samples were capped with Si_3N_4 to prevent oxidation of the surface. An etch mask consisting of cross-linked polymethyl methacrylate (PMMA) was formed on the surface using electron beam lithography and was subsequently developed in acetone. A 300 eV Ar ion mill was used to transfer the etch mask pattern to the $Ni_{80}Fe_{20}$ layer. To prevent oxidation on the sides of the dots, one Si_3N_4-capped sample was covered with 15 nm of ion-beam deposited Al immediately following the ion mill and before breaking vacuum.

Figure 1(a) shows a scanning electron micrograph (SEM) of a 65×71 nm^2 elliptical nanodot array with a 100 nm pitch (center-to-center spacing). Analysis of SEM images yields a standard deviation in dot size of 2 nm. We

[b] Present address: University of Montana, Department of Physics and Astronomy, Missoula, Montana 59812, USA. Electronic mail: michael.schneider@umontana.edu
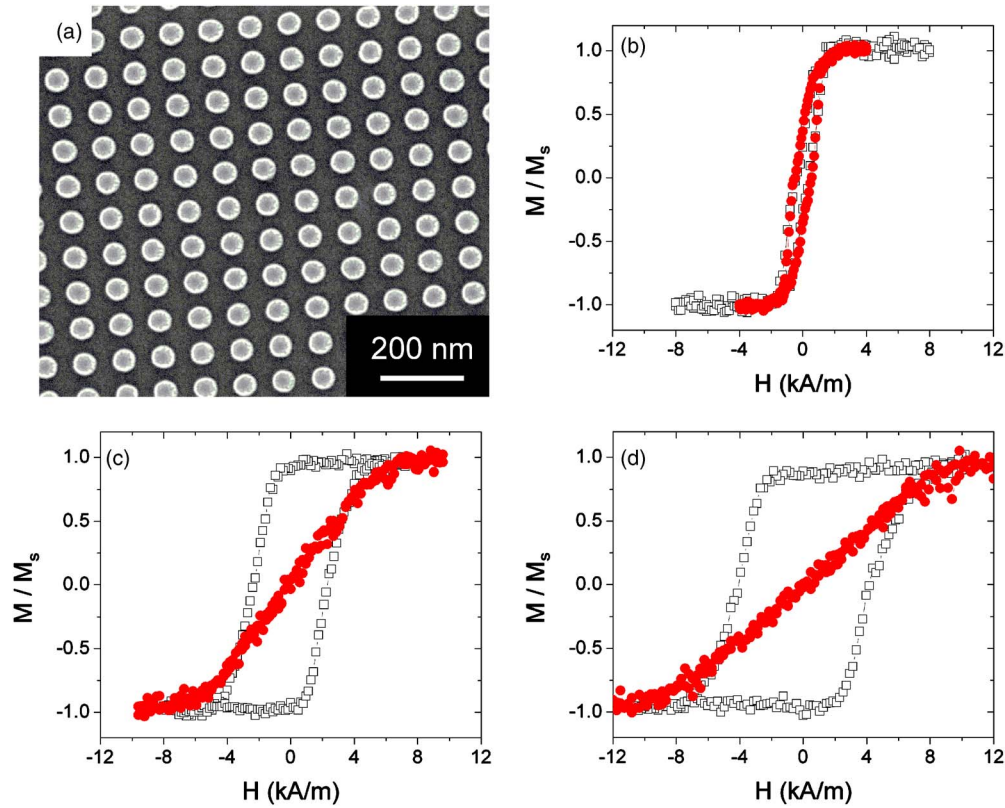
FIG. 1. (Color online) (a) SEM image of 65×71 nm^2 elliptical Permalloy dots. (b) Easy axis (open squares) and hard axis (closed circles) hysteresis loops for an array of circular Permalloy dots, 65×65 nm^2. (c) Easy axis (open squares) and hard axis (closed circles) loops for an array of 5% elliptical Permalloy dots, 65×68 nm^2. (d) Easy axis (open squares) and hard axis (closed circles) loops for an array of 10% elliptical Permalloy dots 65×71 nm^2.

are able to finely adjust the ellipticity of the nanodot arrays in order to adjust the corresponding shape anisotropy and coercivity of the dot arrays. Using conventional MOKE, we measured hysteresis curves along the easy and hard axes to determine the anisotropy field H_k and the coercivity H_c. Figure 1(b) shows the hysteresis curves taken on the nominally 0% ellipticity arrays, i.e., disks. Figures 1(c) and 1(d) shows the hysteresis curves taken on the nominally 5% and 10% elliptical arrays, respectively. The well oriented easy and hard axis behavior of the arrays is indicative of highly ordered arrays of nearly identical nanomagnets. The extracted uniaxial anisotropy H_k was 2.2±0.2, 6.6±0.6, and 9.4±0.9 kA/m for the dot arrays of 0%, 5%, and 10% ellipticity, respectively. The coercivity values H_c were 0.3±0.8, 2.4±1.1, and 4.5±1.7 kA/m for the 0%, 5%, and 10% arrays, respectively, where the error represents the standard deviation of an integrated Gaussian distribution fit. From this dependence of H_c on ellipticity we estimated the dot-to-dot variation from the hysteresis curve and the integrated Gaussian distribution to obtain a switching field distribution. Assuming the curvature is due solely to dot-to-dot variations, this analysis gives an upper limit to the diameter variation of approximately 2 nm standard deviation, consistent with the SEM image analysis.

Figure 2(a) shows typical spectra taken on an array of 65×71 nm^2 Permalloy nanodots at varying applied bias fields, whereas Fig. 2(b) shows typical spectra taken on a Permalloy disk of 20 μm diameter 10 nm thickness that was processed simultaneously and under the same conditions as

the nanodot arrays. The spectra are shown at various applied bias fields. The symbols are the raw data and the lines are the fits described below. In order to fit the resonance curve, we consider the Polder susceptibility tensor as a function of frequency,$\chi(f)$, derived from the Landau-Lifshitz equation of motion for ellipsoidal magnets:[17]

$$\chi(f) = \frac{f_M}{f_0^2 - f^2 - if\Delta f} \begin{bmatrix} (1 + \alpha^2)f_y + i\alpha f & -if \\ if & (1 + \alpha^2)f_x + i\alpha f \end{bmatrix},$$

(1)

where

$$f_0 \doteq \sqrt{f_x f_y} \tag{2}$$

is the resonance frequency,

$$\Delta f \doteq \alpha(f_x + f_y) \tag{3}$$

is the full width at half maximum of the imaginary resonance peak for the diagonal response, α is the damping parameter, $f_{x,y} = |\gamma|\mu_0 H_{x,y}/2\pi$ are the transverse stiffness frequencies, $H_{x,y} \doteq H_b + H_k + (N_{x,y} - N_z)M_s$ are the transverse stiffness fields, $N_{x,y,z}$ are the diagonal components of the demagnetizing tensor, $\gamma = (g\mu_B)/\hbar$ is the gyromagnetic ratio, $g = 2.07$ is the spectroscopic splitting factor, μ_B is the Bohr magneton, $\mu_0 = 4\pi \times 10^{-7}$ H/m is the permeability of free space, H_k is the uniaxial anisotropy field, H_b is the applied field along the z axis, and $f_M = |\gamma|\mu_0 M_s/2\pi$.

The optical measurement geometry detects both polar and longitudinal MOKE signals. Since the dot array is cen-
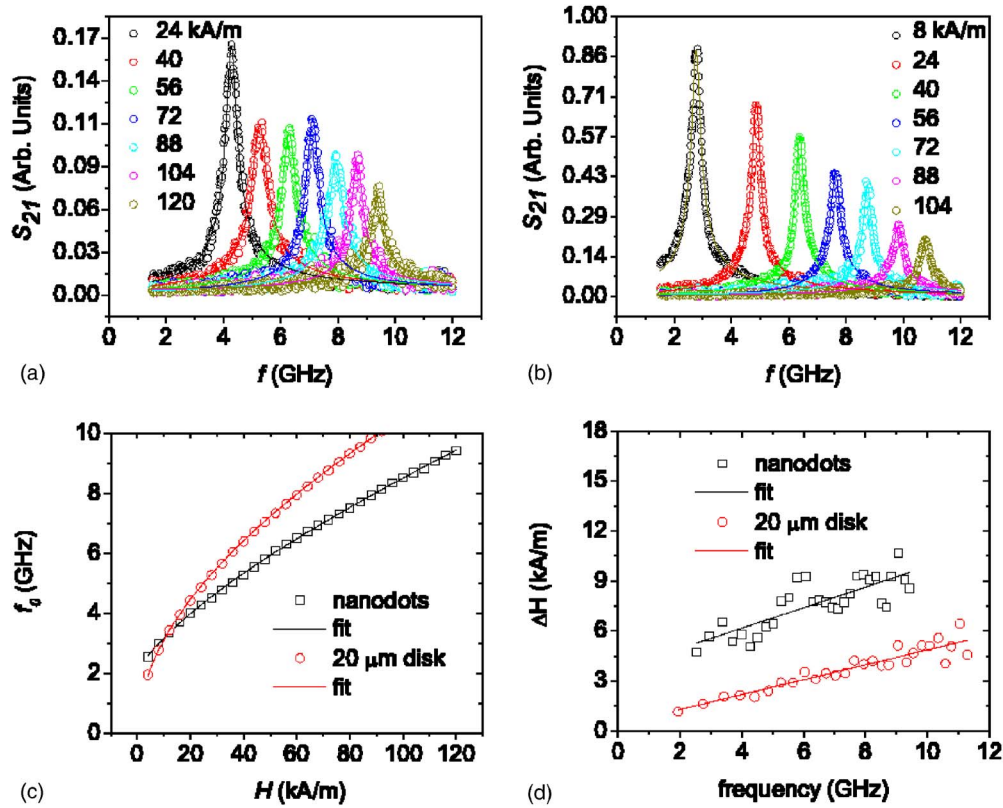
FIG. 2. (Color online) (a) Raw FR-MOKE data (open circles) and fits to Eq. (1) (solid lines) vs frequency for the nanomagnet array at several field values. (b) Raw data (open circles) and fits to Eq. (1) (solid lines) for a 20 μm diameter 10 nm thick Permalloy disk. (c) Resonance frequency vs applied field for 65×71 nm² dots (open squares) and 20 μm diameter 10 nm thick continuous disk (open circles); fits are given by solid lines. (d) Effective field-swept linewidth vs frequency for an array of 65×71 nm² dots (open squares) and 10 nm continuous disk (open circles); fits are shown as solid lines.

tered on the coplanar waveguide used for excitation, we can write the magnitude of the signal transmission parameter S_{21} as

$$|S_{21}| \propto \left| \frac{f_M}{f_0^2 - f^2 - if\Delta f} \right| \sqrt{f_y^2 + (\beta f)^2}, \quad (4)$$

where β is the ratio of the polar to longitudinal MOKE sensitivities. We experimentally determined $\beta = 1.5$ by simultaneously fitting multiple spectra for fields ranging from 4 to 116 kA/m.

Since these nanomagnets are not true ellipsoids, we relied upon the use of an effective demagnetizing tensor N', which we determined by iteratively fitting the frequency versus applied field response. N'_x is the effective demagnetizing component along the axis transverse to the applied field and in the dot plane, N'_y is the effective demagnetizing component perpendicular to the dot plane, and N'_z is the effective demagnetizing component along the applied field direction.

Figure 2(c) shows the resonance frequency versus applied field for both the disk and the array of 65×71 nm² nanodots. The difference between the two responses is expected due to the difference in the shape anisotropy of the ellipses versus the induced uniaxial anisotropy of the continuous disk. We fit the raw data to Eq. (4) assuming $M_s = 800$ kA/m and $H_k = 0.4$ kA/m, which is the growth-induced anisotropy. We then fit the resonance frequency versus field data that we obtained to Eq. (2) in order to obtain H_x and H_y and the N values. We then used these as the values

in Eq. (4) and iterated the fitting process. The values converged after only three iterations: $N'_y - N'_z = 0.504$ and $N'_x - N'_z = 0.010$. If we assume that the sum of these effective demagnetizing factors is approximately equal to 1, then $N'_x = 0.172$, $N'_y = 0.666$, and $N'_z = 0.162$. The demagnetizing factors for the two in-plane directions, N'_x and N'_z, are nearly degenerate, as expected for such dots with nearly equal in-plane axes. The demagnetizing factor of $N'_y = 0.666$ in the thickness axis is equivalent to that for an oblate ellipsoid with a ratio of width to thickness equal to 3.[18] The mode profiles calculated from micromagnetics predict that the precession is concentrated in the ends rather than completely uniform.

Figure 2(d) shows the effective field-swept linewidth for both the continuous disk and the 65×71 nm² array of nanodots. While the overall linewidth of the nanodots is larger than that of the continuous disk, the slope of linewidth versus frequency is approximately the same for both the dots and the continuous disk. This indicates that the damping parameter does not differ strongly between the continuous disk and the nanodots, which is also seen in the fitted value of α of 0.011 ± 0.002 for the nanodots and 0.008 ± 0.001 for the continuous disk. The difference in the overall linewidth can be explained as a larger inhomogeneous contribution to the nanodots, which we find as a zero-frequency intercept of 3.8 ± 0.8 kA/m for the nanodots and 0.4 ± 0.3 kA/m for the continuous disk. We use micromagnetic simulations (de-

scribed in detail below) to quantitatively explain what gives rise to this enhanced inhomogeneous contribution to the linewidth.

III. DISCUSSION

Variation in the FMR frequency from dot-to-dot can arise from fluctuations in the actual dot dimensions. To quantify the degree to which we expect dot-to-dot variations in the dot dimensions to affect linewidth, we performed micromagnetic simulations to determine the sensitivity of the resonance frequency stiffness fields, $H_1 \doteq (N'_x - N'_z)M_s$ and $H_2 \doteq (N'_y - N'_z)M_s$, for individual dots as a function of exact dot size. The dot dynamics were simulated and the resonance frequencies extracted as a function of applied field H_b. The resulting curve was fit to Eq. (2), exactly as was done with the actual data. For nominal 65×71 nm^2 dots we find the variation to be, $\partial H_1/\partial x = 1.76$ (kA/m)/nm, $\partial H_1/\partial y = -2.06$ (kA/m)/nm, $\partial H_2/\partial x = 0.99$ (kA/m)/nm, and $\partial H_2/\partial y = 0.03$ (kA/m)/nm.

Quantitative analysis of SEM micrographs of the dot arrays yields a standard deviation for the lateral dot dimension variations of 2 nm. The films used to fabricate the nanodots are sufficiently flat that we can ignore dot-to-dot thickness variations. Thus, we calculate the standard deviation of stiffness field fluctuations for uncorrelated dimensional variations and get $\sigma H_1 \approx 5.4$ kA/m and $\sigma H_2 \approx 2.1$ kA/m. Error analysis shows that the standard deviation of the resonant field distribution is given by

$$\sigma_H = \frac{H_b + H_2}{2H_b + H_1 + H_2}\sigma H_1 + \frac{H_b + H_1}{2H_b + H_1 + H_2}\sigma H_2. \qquad (5)$$

The linewidth (full width at half maximum) associated with these Gaussian resonant field distributions is $\Delta H'_0 = 2(2\ln 2)^{1/2}\sigma_H$. Since Eq. (5) depends on applied field, it is important to note that inhomogeneous broadening effects will generally affect both the slope and intercept of frequency-linewidth versus frequency data, as will be explained below.

Using Eq. (5), we can estimate how a variation in dot dimension of 2 nm will affect the extracted damping and zero-frequency–linewidth intercepts. We begin by calculating field-swept linewidth, using the expression

$$\Delta H = \frac{4\pi\alpha f}{\gamma\mu_0}, \qquad (6)$$

with a damping value of $\alpha = 0.008$. Then, using Eq. (5), we can estimate the effective linewidth intercept and effective damping by fitting the sum of Eqs. (5) and (6) to the inhomogeneous linewidth model given by

$$\Delta H_{\text{eff}} = \Delta H'_0 + \frac{4\pi\alpha' f}{\gamma\mu_0}. \qquad (7)$$

Using linear regression to fit our calculated data, we obtained $\Delta H'_0 = 13.2$ kA/m and $\alpha' = 0.006$, while our experimental re-

sults are $\Delta H_0 = 3.8 \pm 0.8$ kA/m and $\alpha = 0.011 \pm 0.002$. The measured inhomogeneous resonance line broadening is much less than what we predicted based on dimensional variations, while the α value is larger. Part of this difference may be accounted for by dipolar coupling between the dots. A simple estimate yields 4.6 kA/m maximum dipole fields due to a nearest-neighbor dot. Note that if the dot-to-dot variation was only 1 nm, we would be closer to agreement between the predicted values and the experiment. For a 1 nm uncorrelated dot-to-dot variation, we would expect $\Delta H_0 = 6.6$ kA/m and $\alpha = 0.007$.

It has been suggested that there is an increase in damping due to the native oxide that is present in the standard lithography and is present in other nanopillar systems.[6–8] However, we fabricated dots that were encapsulated in 12 nm of Al before exposure to ambient air to prevent oxidation. We also fabricated samples that were capped with Si$_3$N$_4$ on the top surface but had bare side walls. We found no significant difference in the extracted damping parameter with or without Al encapsulations or Si$_3$N$_4$ capping. There was also no significant difference in the resonance frequency at a given field between the encapsulated, capped, and air-exposed samples.

IV. CONCLUSION

In conclusion, we developed a technique to directly probe the ferromagnetic resonance of arrays of 65×71 nm^2 nanomagnets. The effective damping in these dots is comparable to that of thin films of the same material. In addition, the effective shape anisotropy is in agreement with micromagnetic simulations of this particular dot geometry. By comparison of the data with micromagnetic simulations, we conclude that dot-to-dot size variations lead to a linewidth broadening that can be seen as a nonzero intercept in the ΔH versus f plot. The results of the micromagnetic simulations and our experimental results indicate that, while we cannot rule out a modest increase in damping for single-dot dynamics due to processing, dot-to-dot size inhomogeneties on the order of only 1 nm can significantly broaden the effective linewidth for arrays of nanodots.

[1]M. D. Stiles and J. Miltat, in *Spin Dynamics in Confined Magnetic Structures III*, edited by B. Hillebrands and A. Thiaville (Springer, Berlin, 2006).

[2]T. Thomson, G. Hu, and B. D. Terris, Phys. Rev. Lett. **96**, 257204 (2006).

[3]S. H. Chung, A. Hoffmann, S. D. Bader, C. Liu, B. Kay, L. Makowski, and L. Chen, Appl. Phys. Lett. **85**, 2971 (2004).

[4]E. A. Anderson, S. Isaacman, D. S. Peabody, E. Y. Wang, J. W. Canary, and K. Kirshenbaum, Nano Lett. **6**, 1160 (2006).

[5]R. A. McMillan, C. D. Paavola, J. Howard, S. L. Chan, N. J. Zaluzec, and J. D. Trent, Nat. Mater. **1**, 247 (2002).

[6]J. C. Sankey, P. M. Braganca, A. G. F. Garcia, I. N. Krivorotov, R. A. Buhrman, and D. C. Ralph, Phys. Rev. Lett. **96**, 227601 (2006).

[7]D. Lacour, J. A. Katine, N. Smith, M. J. Carey, and J. R. Childress, Appl. Phys. Lett. **85**, 4681 (2004).

[8]N. C. Emley, I. N. Krivorotov, O. Ozatay, A. G. F. Garcia, J. C. Sankey, D. C. Ralph, and R. A. Buhrman, Phys. Rev. Lett. **96**, 247204 (2006).

[9]P. M. Braganca, I. N. Krivorotov, O. Ozatay, A. G. F. Garcia, N. C. Emley, J. C. Sankey, D. C. Ralph, and R. A. Buhrman, Appl. Phys. Lett. **87**, 112507 (2005).

[10]B. Heinrich, Y. Tserkovnyak, G. Woltersdorf, A. Brataas, R. Urban, and G. E. W. Bauer, Phys. Rev. Lett. **90**, 187601 (2003).

[11]Y. Tserkovnyak, A. Brataas, and G. E. W. Bauer, Phys. Rev. B **67**, 140404

(2003).

[12]I. N. Krivorotov, N. C. Emley, J. C. Sankey, S. I. Kiselev, D. C. Ralph, and R. A. Buhrman, Science **307**, 228 (2005).

[13]M. Pardavi-Horvath, C. A. Ross, and R. D. McMichael, IEEE Trans. Magn. **41**, 3601 (2005).

[14]A. Barman, S. Q. Wang, J. D. Maas, A. R. Hawkins, S. Kwon, A. Liddle, J. Bokor, and H. Schmidt, Nano Lett. **6**, 2939 (2006).

[15]S. S. Kalarickal, P. Krivosik, M. Wu, C. E. Patton, M. L. Schneider, P. Kabos, T. J. Silva, and J. P. Nibarger, J. Appl. Phys. **99**, 093909 (2006).

[16]S. Yabukami, M. Yamaguchi, K. I. Arai, M. Watanabe, A. Itagaki, and H. Ando, J. Appl. Phys. **85** 5148 (1999).

[17]C. E. Patton, in *Magnetic Oxides*, edited by D. J. Craik (Wiley, London, 1975), p. 575.

[18]R. M. Bozorth, in *Ferromagnetism* (Wiley, New York, 1993), p. 849.